PAPER

All-optical spatio-temporal metrology for isolated attosecond pulses

IOP Publishing Journal of Physics B: Atomic, Molecular and Optical Physics
J. Phys. B: At. Mol. Opt. Phys. **55** (2022) 205601 (9pp) https://doi.org/10.1088/1361-6455/ac8f01

All-optical spatio-temporal metrology for isolated attosecond pulses

Lixin He[1,2], Jianchang Hu[1], Siqi Sun[1], Yanqing He[1], Yu Deng[1], Pengfei Lan[1,2,*] and Peixiang Lu[1,2,3]

[1] Wuhan National Laboratory for Optoelectronics and School of Physics, Huazhong University of Science and Technology, Wuhan 430074, People's Republic of China
[2] Optical Valley Laboratory, Hubei 430074, People's Republic of China
[3] Hubei Key Laboratory of Optical Information and Pattern Recognition, Wuhan Institute of Technology, Wuhan 430205, People's Republic of China

E-mail: pengfeilan@hust.edu.cn

Received 23 June 2022, revised 25 August 2022
Accepted for publication 31 August 2022
Published 20 September 2022

Abstract

Characterizing an isolated attosecond pulse (IAP) is essential for its potential applications. A complete characterization of an IAP ultimately requires the determination of its electric field in both time and space domains. However, previous methods, like the widely-used RABBITT and attosecond streaking, only measure the temporal profile of the attosecond pulse. Here we demonstrate an all-optical method for the measurement of the space-time properties of an IAP. By introducing a non-collinear perturbing pulse to the driving field, the process of IAP generation is modified both spatially and temporally, manifesting as a spatial and a frequency modulation in the harmonic spectrum. By using a FROG-like retrieval method, the spatio-spectral phases of the harmonic spectrum are faithfully extracted from the induced spatio-spectral modulations, which allows a thorough characterization of the IAP in both time and space. With this method, the spatio-temporal structures of the IAP generated in a two-color driving field in both the near- and far-field are fully reconstructed, from which a weak spatio-temporal coupling in the IAP generation is revealed. Our approach overcomes the limitation in the temporal measurement in conventional *in situ* scheme, providing a reliable and holistic metrology for IAP characterization.

Keywords: isolated attosecond pulse, spatio-temporal characterization, all-optical metrology

(Some figures may appear in colour only in the online journal)

1. Introduction

The advent of attosecond extreme ultraviolet/soft x-ray pulses via high-order harmonic generation (HHG) is a milestone in strong-field physics and attoscience [1–8], which has opened up new avenues for accessing ultrafast electron dynamics in atoms [9–12], molecules [13–15], and condensed matter [16] on its natural time scale. HHG is a highly nonlinear process during the laser-matter interaction [17–19], accompanying with complicated macroscopic effects in the propagation [20–22]. Isolated attosecond pulses (IAPs) produced by HHG generally have complex spatio-temporal structures, which encode both the ångstrom-sized spatial features and attosecond scale temporal features of the response of the matters to the laser field. A complete characterization of the IAP in both time and space is critical not only for the development of new attosecond light sources, but also for its applications in attosecond pump-probe experiments, as well as for unraveling the physics underlying the laser-matter interaction [23–25].

The complete characterization of an ultrashort IAP actually requires the determination of its spatio-temporal electric field $E(x, y, t)$, or its spatio-spectral counterpart $\tilde{E}(x, y, \omega)$. To date, attosecond streaking technique [26, 27] has been usually used to retrieve the temporal profile of an IAP from

* Author to whom any correspondence should be addressed.

the streaked photoelectron spectrogram of atoms with the (frequency-resolved optical gating for complete reconstruction of attosecond bursts) algorithm [28–31]. Several other methods, such as the phase retrieval by omega oscillation filtering [32], Volkov transform generalized projection algorithm [33], the genetic algorithms [34–36], and the neural networks [37, 38], have also been developed to overcome the theoretical and experimental limitations in the attosecond streaking technique, e.g., the assumption of central momentum approximation and the high statistic noise in the streaking trace due to the low photon flux of the attosecond pulse. However, all these temporal characterization approaches rely on the conversion of the attosecond pulse into electron wavepackets through photoionization of atoms, which have automatically averaged the spatial structure of the IAP in the measurement. Considering the possible significant space-time coupling in the highly nonlinear generation process of IAP [39, 40], the temporal measurement averaged over the space will be inadequate in many cases. Although some approaches, such as, the point-diffraction interferometry [41], the spectral wavefront optical reconstruction by diffraction [42], and the lateral shearing interferometry [43], have been demonstrated for the spatial characterization of high-order harmonics, none of them is compatible with the temporal measurement.

On the other hand, an *in situ* method based on a weak perturbation of the harmonic generation process by a second-harmonic field that co-propagates with the fundamental beam was introduced [44]. In this scheme, the temporal information of attosecond pulse was decoded from the two-color delay-dependent modulations of the generated even-harmonics. Later on, Kim *et al* reformed this *in situ* method with the weak perturbing beam propagating non-collinearly with the driving beam [45]. This configuration built a spatial gating as the two-color delay varies, allowing a synchronous measurement of the spatial and temporal characteristics of the attosecond pulse. However, in this *in situ* scheme, a linear spectral group delay dispersions (GDD) of the emitted harmonics were assumed and derived from the spatial modulation of the far-field harmonic signals. More complex spectral phase information, such as high-order dispersion in the IAP, is critical for the temporal measurement but is unavailable with this scheme.

In this work, we demonstrate an improved *in situ* approach for accurate measurement of the spatio-temporal structures of an IAP. We find that in addition to the spatial modulation, the utilization of the weak perturbing beam can also lead to a frequency (temporal) modulation in the harmonic generation as its time delay varies. With a method similar to the phase retrieval of femtosecond laser with the frequency-resolved optical gating (FROG) technique [46], the spatial and spectral harmonic phases are successfully extracted from the spatial and frequency modulations of the generated harmonics, respectively. This allows us to build the spatio-spectral connection of the harmonic phase and then achieve a complete characterization of IAPs in both time and space. Our method obviates the linear GDD approximation in conventional *in situ* measurement [45], allowing an exact characterization of the IAP. With this method, we have demonstrated a full spatio-temporal reconstruction of the IAP generated by a two-color driving field in experiment. The spatio-temporal coupling effect during the IAP generation is revealed from the reconstructions.

2. Methods

2.1. Principle of the spatio-temporal characterization of an IAP

For the spatio-temporal characterization of an IAP, we imitate the spatially encoded *in situ* method in [45] by introducing a weak perturbing beam to modify the HHG process both spatially and temporally. In space, the perturbing beam could alter the wavefront of HHG in the near-field, which, in turn, will modify the far-field spatial distribution of the harmonic spectrum. By scanning the time delay between the perturbing and driving lasers, spatial modulations in the far-field distributions of the harmonics can been observed. In our experiment (see figure 1(a)), the lasers have a transverse spatial distribution in the (x, y) plane normal to the propagation direction z. Only the vertical component of the far-field pattern of the harmonic spectrum is measured due to the use of an entrance slit along the y direction. Based on the strong field approximation theory [18, 44, 45], the spatial modulation induced by the perturbation in our experiment can be approximated as

$$|E_{\mathrm{far}}(\omega,\theta,\tau)|^2 \approx |\int E_{\mathrm{near}}(\omega,y,\tau)G(y-c\tau/\vartheta)e^{ik_\omega\theta y}\,dy|^2, \tag{1}$$

where E_{far} and E_{near} are spatially-resolved complex amplitude of the harmonic with the frequency of ω in the far- and near-field, respectively. The modulus squares of E_{far} and E_{near} represent the distributions of the harmonic in space. y is the spatial coordinate in the near-field, θ is the divergence of the harmonic in the far-field, τ and ϑ are the time delay and crossing angle between the perturbing and driving lasers, respectively. k_ω is the wavenumber of the harmonic, c is the speed of the light. $G(y-c\tau/\vartheta)$ is a spatial gate induced by the perturbing pulse, which represents the modifications in both the amplitude and phase of E_{near}. Note that, in equation (1), only the short quantum trajectory is considered due to its better phase matching in our experiment. Besides, in our experiment, an entrance slit along the y-axis was installed (see below). We observe the far-field HHG pattern as a thin vertical slice in the y direction after the harmonic beam passes through the entrance slit. The horizontal component was not observed in our experiment. So in equation (1), the angle for the horizontal (x) direction has been set to zero. In this case, reconstructing the spatial structure of the unperturbed harmonics (E_{near}) is equivalent to solving the retrieval problem of femtosecond laser pulses with the FROG technique [46], where the unperturbed harmonics (E_{near}) is equivalent to the 'pulse' to be measured, and $G(y-c\tau/\vartheta)$ is equivalent to the 'gate' in the FROG technique. In this work, we have used the standard FROG algorithm, i.e., the widely-used principal

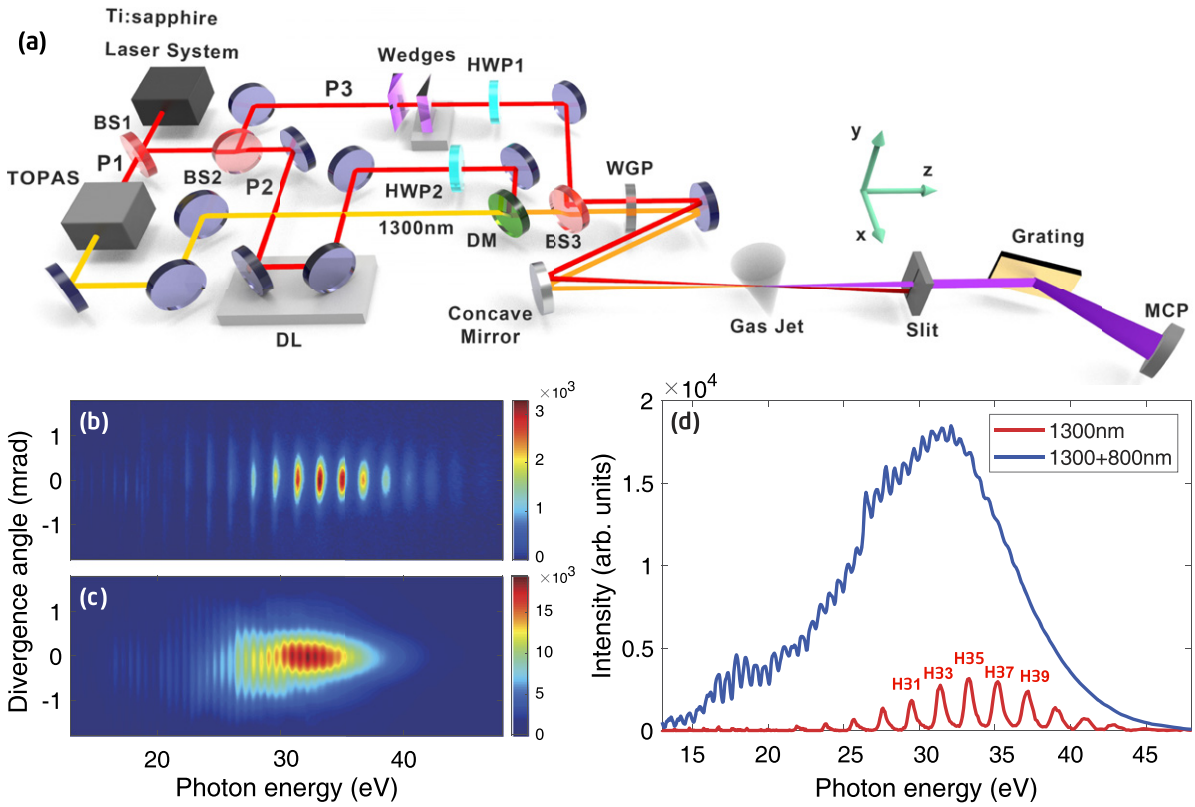

Figure 1. (a) Schematic diagram of the experimental set-up for the spatio-temporal measurement of the IAP generated in a tow-color driving field. BS, beam splitter; DM, dichroic mirror; DL, delay line; HWP, half-wave plate; WGP, wire grid polarizer. (b) Spatially-resolved harmonic spectrum driven by the 1300 nm fundamental field alone. (c) Same as (b), but for the two-color driving field synthesized by the 1300 nm fundamental and 800 nm assistant laser fields. (d) On-axis harmonic spectra driven by the one-color (red line) and two-color (blue line) laser field, respectively.

component generalized projection algorithm (PCGPA) [47], to extract the unperturbed harmonics (E_{near}) and the spatial gate $G(y - c\tau/\vartheta)$ from the delay-dependent far-field patterns of the harmonics. In the reconstruction, we first give random initial guesses of the 'pulse' and 'gate' and suppose the 'pulse' and 'gate' are sampled with a constant spacing in time (or space). Then the 'pulse' and 'gate' can be thought of as vectors with the elements sampled at discrete times. With the vectors of the 'pulse' and 'gate', we can construct an outer product matrix of these two vectors. A one-to-one transformation via permutations then converts the outer product into a time-domain trace of the initial guess. By Fourier transforming each column of the guessed time-domain trace and meanwhile applying the experimental trace as an intensity constraint, we can obtain a new frequency domain trace. The new frequency domain trace is further transformed back to the time domain. With an inverse of the outer-product-to-time-domain transform, an outer product 'form' matrix is generated. The 'form' matrix is further decomposed into a superposition of weighted outer products by the singular value decomposition [47]. The vector pair (outer product) with the largest corresponding weight is the best rank one approximation of the outer product form in the least squares sense, which is used as the initial values for the next iteration. The above process is repeated until the RMSE between the generated and measured trace reaches 10^{-6}.

The second step is to determine the temporal properties of the IAP. In this regard, it needs to know the relative spectral phase of the whole spectrum. In [45], this relative spectral phase has been defined as the linear group delay in HHG, and was directly acquired from the delay-dependent spatial modulations of harmonics with different photon energies. This manner ignores more complex phase information in the IAP, which will limit the accuracy of the temporal measurement. Here we demonstrate an improved method for accurate temporal measurement. We find that, in addition to the spatial modulation, the introduced weak perturbing pulse can also lead to a modulation in the HHG process in the time domain, i.e.,

$$d(t,\tau) = d_0(t)g(t,\tau) + \text{c.c.} \tag{2}$$

where $d_0(t)$ denotes the dipole moment without the perturbation, $g(t,\tau)$ is the modulation induced by the perturbing pulse. In previous works [44, 48], it was usually assumed that the weak perturbing pulse will not affect the ionization process, but mainly perturbs the free electron's actions in the laser field. Then the induced modulations can be approximated as $g(t,\tau) = e^{-i\sigma(t,\tau)}$, where $\sigma(t,\tau)$ is the additional phase induced by the perturbing pulse. In this work, the influences of the perturbing pulse on both the dipole amplitude and phase have been taken into account. That means $g(t,\tau)$ in our reconstruction is a complex-valued quantity. The harmonic spectrum then can

be obtained by

$$S(\omega,\tau) = \omega^4 \left| \int d_0(t) g(t,\tau) e^{i\omega t}\, dt \right|^2. \quad (3)$$

Equation (3) indicates that the weak perturbing pulse introduces a temporal phase gate in the harmonic generation, which will lead to a frequency modulation in the harmonic spectrum. Reformulating equation (3), we can get

$$\frac{S(\omega,\tau)}{\omega^4} = \left| \int d(t,\tau) e^{i\omega t}\, dt \right|^2 = \left| \int d_0(t) g(t,\tau) e^{i\omega t}\, dt \right|^2. \quad (4)$$

Equation (4) is also equivalent to the equation used in FROG technique. With the PCGPA method mentioned above, we can also retrieve the unperturbed complex dipole moment $d_0(t)$ and then the spectral phase from the frequency-modulated harmonic spectra. With both the spatial and spectral phases reconstructed, we can then achieve a full characterization of the IAP in both time and space.

2.2. Experimental method

In our work, to obtain an IAP, we adopted a two-color driving field, which is synthesized by a 1300 nm fundamental field and an 800 nm assistant field, to generate high-order harmonics. A schematic diagram of the experimental setup is shown in figure 1(a). To be specific, the output of a commercial Ti: sapphire laser system (Astrella-USP-1K, Coherent, Inc.), which delivers 33 fs, 800 nm pulses at a repetition rate of 1 kHz, with the maximum pulse energy of 7 mJ, was divided into three beams by two 30% reflection beam splitters (BS1 and BS2). The transmitted beam P1 after BS1 with the energy of 4.9 mJ was employed to pump an optical parametric amplifier (TOPAS-Prime-Plus, Coherent) to generated a 60 fs, 1300 nm fundamental driving laser. The transmitted 800 nm laser P2 after BS2 was recombined with the 1300 nm laser by a dichroic mirror as an assistant field to synthesize the two-color driving field. A motorized delay line was installed in the arm of P2 to control the relative phase of the two-color field.

A weak 800 nm laser P3 reflected by BS2 was introduced as a perturbing beam to modify the HHG process. The two-color driving field and the perturbing beam were recombined by BS3 and focused non-collinearly (the crossing angle is about 15 mrad) onto a gas jet to generate high-order harmonics by a $f = 20$ cm concave mirror. The diameter of the focal spot is estimated to be 60 μm. In our experiment, we chose argon atom as the prototype to demonstrate our scheme. The background gas pressure is about 20 Torr. The gas jet is placed at 1 mm after the laser focus to ensure the phase matching of the short quantum trajectory. A wire grid polarizer (WGP) was inserted after BS3 to ensure the same polarization direction of all these pulses. In combination with the WGP, two half-wave plates (HWPs) were installed in the arms of P2 and P3 to adjust their intensities. A pair of wedges were installed in the arm of P3 to adjust the time delay between the perturbing pulse and the two-color field.

The generated high-order harmonics were detected by a homemade flat-field soft x-ray spectrometer, which consists of a 0.2 mm-wide, 15 mm-height entrance slit, a flat-field grating (1200 grooves mm^{-1}), and a microchannel plate backed with a phosphor screen. A charge-coupled device camera is used to record the spectrally resolved images.

3. Results and discussion

Figure 1(b) plots the measured far-field pattern of the harmonic spectrum driven by the 1300 nm fundamental laser alone. One can see clear discrete odd harmonics with the photon energy up to 45 eV [47th harmonic (H47)] in the spectrum (see red line in figure 1(d)). While in the two-color driving scheme, by optimizing the intensity and relative phase of the 800 nm assistant field with respect to the 1300 nm fundamental field, a smooth supercontinuum in the region of 33–45 eV is obtained (see figures 1(c) and (d)), which can support the generation of an IAP in the experiment. The discrete and continuous harmonics in the one-color and two-color laser field can be well understood by the classical simulations (not presented here) based on the three-step model [17]. In the one-color laser field, the harmonics are generated within each half optical cycle. The interference of the each half cycle radiation thus leads the discrete harmonics in the spectrum. Moreover, in the one-color field, the maximum photon energy of half-cycle radiation that contributes to harmonic cutoff is very close to that of its adjacent half-cycle radiations. Thus it is difficult to generate a continuous spectrum in the one-color field. While in the two-color field, the energy difference between the highest and its adjacent half-cycle radiations is enlarged by the 800 nm assistant field. Moreover, after the macroscopic propagation, the short trajectory of the highest radiation is selected. Thus a continuous spectrum is generated in the energy range (33–45 eV) in our two-color experiment. Small modulation that appears in the range of 13–33 eV is due to the existence of satellite radiations beside the main pulse as in [49, 50]. Moreover, as shown in figure 1(d), the HHG yield in the two-color field (blue line) is visibly enhanced (by $\sim$5 times) compared to that in the one-color field (red line). This, on the one hand, is due to the increase of the ionization rate induced by the 800 nm assistant field. On the other hand, in the two-color field, the released electrons spend shorter time in the continuum, which reduces the wave-packet spreading in the HHG process. Such a trajectory shortening effect will also contribute to the increase of the HHG yield [51, 52].

Figure 2(a) shows the far-field spatial distributions of H35 measured in the two-color laser field as a function of the time delay between the perturbing and driving laser pulses. One can see clear modulations in the far-field distribution of the harmonic as the time delay varies. According to equation (1), the unperturbed complex harmonic amplitude in the near-field as well as the spatial gate induced by the perturbing beam can be uniquely extracted from the FROG-like trace in figure 2(a) by using the PCGPA method.

Figure 2(b) displays the PCGPA reproduction of the far-field pattern of H35 as a function of time delay of the perturbing pulse. The result agrees well with the experimental

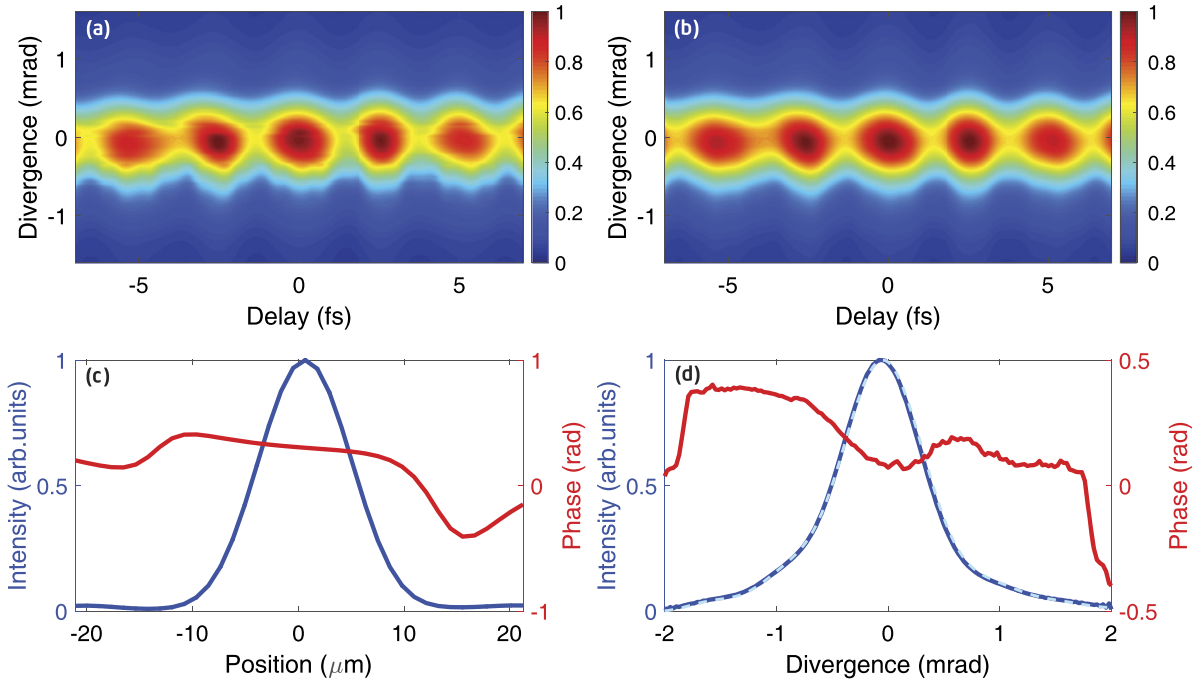

Figure 2. (a) Far-field spatial distribution of H35 as a function of time delay of the perturbing laser. (b) Same as (a), but for the PCGPA reconstruction. (c) Reconstructed near-field distribution of the intensity (blue line) and phase (red line) of H35. (d) Reproduced far-field intensity (blue line) and phase (red line) of H35. The cyan dashed line plots the measured far-field intensity of the unperturbed H35 for comparison.

measurement shown in figure 2(a). Figure 2(c) plots the reconstructed distributions of the intensity (blue line) and phase (red line) of the unperturbed H35 in the near-field. With the reconstructed near-field result, we can further obtain the far-field distribution of the unperturbed harmonic in terms of

$$E_{\text{far}}(\omega,\theta) = \int E_{\text{near}}(\omega,y)e^{ik_\omega\theta y}\,dy. \tag{5}$$

The reconstructed far-field results are plotted in figure 2(d). For comparison, we have also performed HHG experiment without the perturbation. The measured far-field distribution of the intensity of H35 is plotted as the cyan dashed line in figure 2(d), which shows good agreement with the reconstruction (blue solid line), proving the validity of our reconstruction. Repeating the above procedure for each photon energy, we can then achieve the spatial measurement of both the amplitude and phase of the whole harmonic spectrum in both the near- and far-field.

Secondly, we demonstrate the temporal measurement of the generated IAP. To this end, it requires to determine the relative spectral phase of the whole harmonic spectrum. Our method relies on the frequency (temporal) modulation induced by the perturbing laser in the harmonic generation. As shown in figure 3(a), by scanning the time delay between the perturbing and driving laser fields, one can see clear modulations in the 2D spectrogram of the far-field on-axis harmonic spectrum. Similar result is also found for the harmonic spectra at other spatial positions (not presented here). According to equation (4), we can retrieve the unperturbed complex harmonic dipole moment $d_0(t)$ and then the spectral phase of the harmonic spectrum from the measured 2D spectrogram trace by using the PCGPA method.

In figure 3(b), we plot the PCGPA reproduction of the spectrogram trace of the far-field on-axis harmonic spectrum. As shown, the reconstruction agrees well with the measurement in figure 3(a). Figure 3(c) displays the reconstructed unperturbed spectral intensity (blue solid line) and phase (red dotted line) of the on-axis harmonic spectrum in the far field. The reconstructed spectral intensity is also in good agreement with the unperturbed measurement (cyan dashed line). In the supercontinuum, with the photon energy varying from 33 eV to 47 eV, the harmonic phase has changed by 0.75 rad, corresponding to a 320 as difference in the emission times of these harmonics. Besides, one can see that the spectral phase is irregular in the energy range from 13 eV to 33 eV. This complicated phase variation mainly arises from the interference of the multiple half-cycle radiations in this energy range, which deviates far from the linear group delay defined in [45], indicating a complex dispersion in this energy range. This complex dispersion cannot be measured with the method in [45]. By connecting the retrieved spectral phase and the spatial reconstructions above, the intensity and phase of the far-field harmonics then can be fully determined in the whole space. The near-field result can also be obtained by performing inverse Fourier transform of the far-field result. Note that the relative spectral phase in principle can be retrieved from the harmonic spectrum measured at each spatial position in the far-field. Owing to the experimental errors in the measurement, the phase connection built at different spatial positions may be discrepant. In this work, we have retrieved the spectral phase from the far-field harmonic spectra in the range from -0.5 to 0.5 mrad,

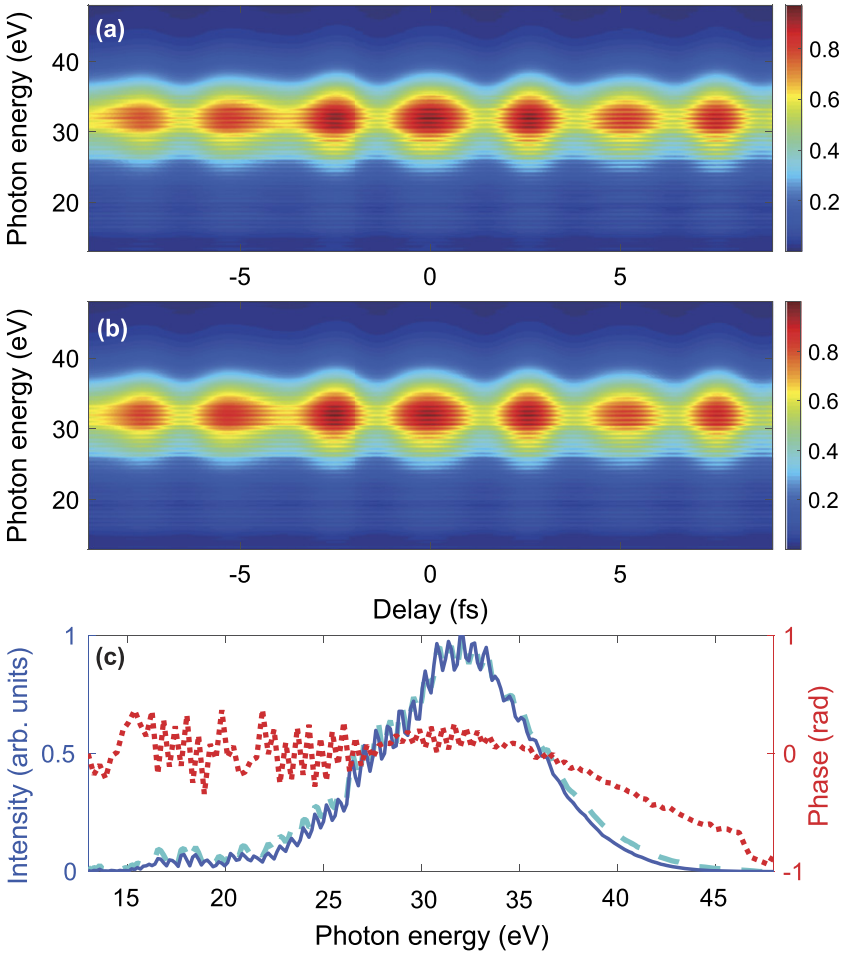

Figure 3. (a) On-axis harmonic spectra measured in the two-color driving field as a function of time delay of the perturbing laser. (b) Same as (a), but for the PCGPA reconstruction. (c) Reproduced intensity (blue solid line) and phase (red dotted line) of the unperturbed on-axis harmonic spectrum in the far-field. The cyan dashed line plots the far-field on-axis harmonic intensity measured without the perturbation for comparison.

and then optimized the spatio-spectral phase connection from the retrievals by minimizing the difference between the measurement and the reconstruction with a surrogate-based optimization algorithm [53]. Figure 4 shows the reconstructed distributions of the harmonic intensity (figures 4(a) and (c)) and phase (figures 4(b) and (d)) in both the far- and near-field.

With the reconstructed harmonic amplitudes and phases in figure 4, we can finally achieve a spatio-temporal measurement of the IAP by superposing the harmonics in the supercontinuum (33–47 eV) coherently. Figure 5(a) shows the electric field of the far-field attosecond pulse as a function of the time and position. The inset plots the spatio-temporal profile of the pulse intensity. The pulse duration of the on-axis emission is measured to be 270 as (figure 5(b)). The results in the near-field are also shown in figures 5(c) and (d). The duration of the on-axis attosecond pulse in the near-field is about 243 as, which is slightly shorter than the far-field result.

For a quantitative characterization of the spatio-temporal structure of the generated IAP, we have further calculated the normalized spatial chirp $\rho_{y\omega}$ of the IAP in both the near- and far-field in terms of [54, 55]

$$\rho_{y\omega} = \frac{\iint y\omega I(y,\omega)dy\,d\omega}{\sqrt{\iint y^2 I(y,\omega)dy\,d\omega \iint \omega^2 I(y,\omega)dy\,d\omega}}, \tag{6}$$

where $I(y,\omega)$ denotes the spatio-spectral distribution of the harmonic intensity in figures 4(a) and (c). Similarly, the normalized pulse front tilt ρ_{yt} is also evaluated from the spatio-temporal distributions $I(y,t)$ of the IAP in figures 5(a) and (c) according to

$$\rho_{yt} = \frac{\iint yt I(y,t)dy\,dt}{\sqrt{\iint y^2 I(y,t)dy\,dt \iint t^2 I(y,t)dy\,dt}}. \tag{7}$$

The normalized spatial chirp $\rho_{y\omega}$ of the IAP generated in the near- and far-field in our two-color experiment are calculated to be -0.006 and 0.034, respectively. The normalized front tilts retrieved for the near- and far-field IAP are -0.023 and 0.014. Both the spatial chirp and front tilt of the generated IAP are very small, indicating a weak spatio-temporal distortion of the IAP in our experiment. The slight difference between the near- and far field results reveals a weak spatio-temporal coupling during the macroscopic propagation in our experiment.

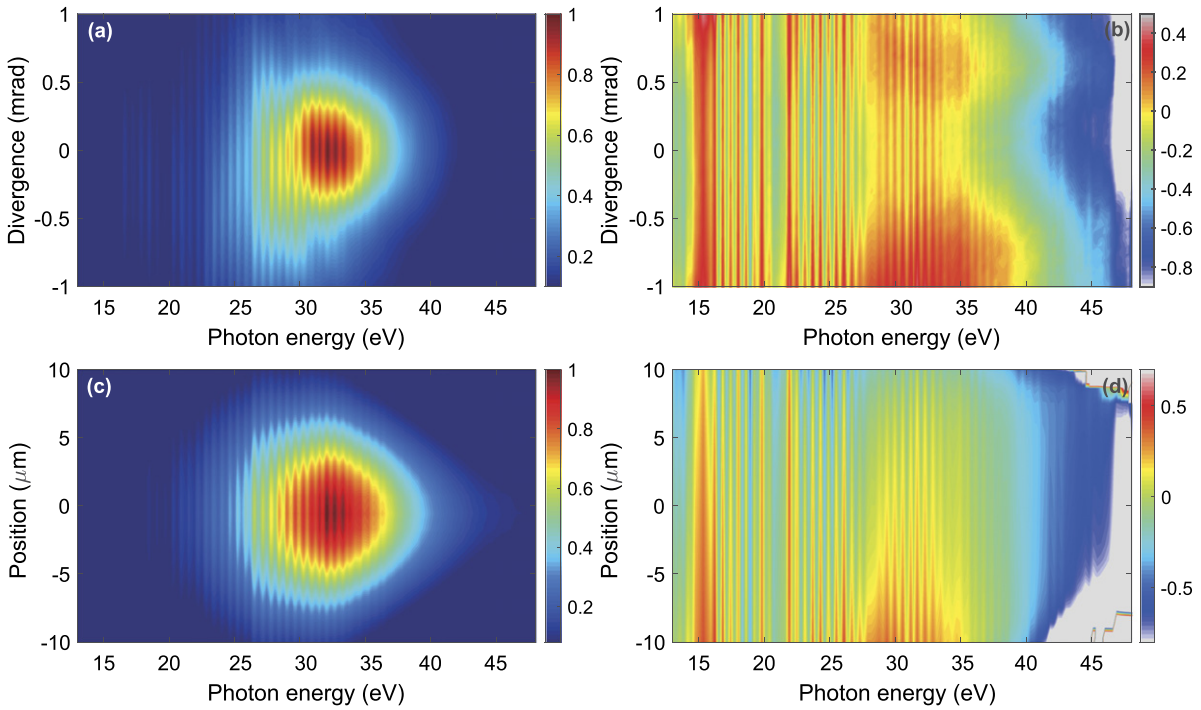

Figure 4. (a) and (b) Spatially-resolved far-field harmonic intensity (a) and phase (b) reconstructed from the measurement. (c) and (d) Same as (a) and (b), but for the near-field result.

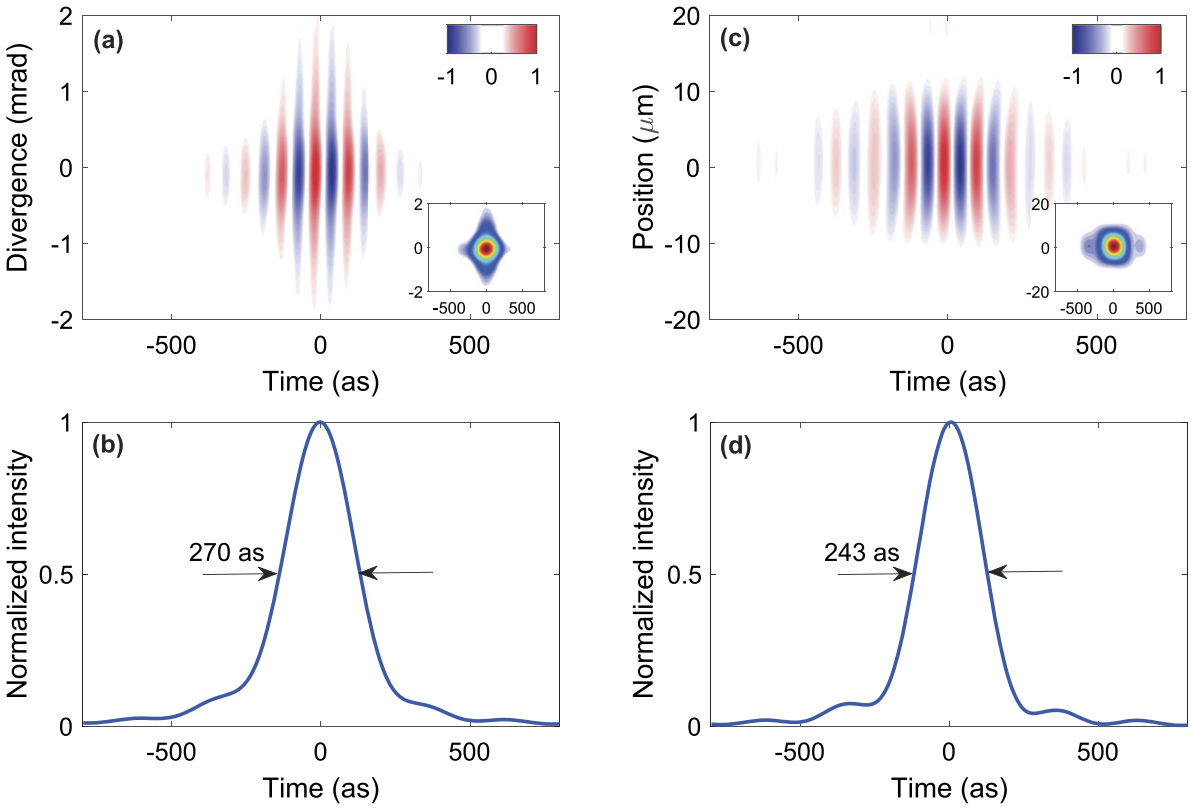

Figure 5. (a) Spatio-temporal profiles of the electric field of the attosecond pulse in the far-field obtained by synthesizing harmonics in the energy range from 33 eV to 47 eV. The inset shows the corresponding spatio-temporal distribution of the intensity of the attosecond pulse. (b) Temporal profile of the on-axis attosecond pulse in the far field. (c) and (d) Same as (a) and (b), but for the near-field result.

It can be expected that the spatio-temporal coupling will be more prominent for a highly-ionized dense gas medium, where the nonlinear propagation effect becomes more significant [39, 40]. In this case, the driving laser may be severely distorted by the propagation effects. Then the single-atom dipole $d_0(t)$ in equations (2)–(4) will be modified. Since our reconstruction method is based on the modulations induced by the perturbing pulse in both time and space, although the single-atom dipole is modified, the modulations induced by the perturbing pulse can still hold after propagation. Thus our reconstruction method can still work. But the retrieved harmonic dipole should be the modified one induced by the distorted driving laser.

4. Conclusion

In conclusion, we have introduced an all-optical *in situ* method for the complete spatio-temporal characterization of IAPs. Our scheme relies on the weak perturbations induced by the perturbing laser on the HHG process in both time and space, which results in a spatial and also a frequency modulation in the far-field harmonic spectrum. From these modulations, the spatial and spectral phases of the harmonics can be accurately extracted by using a FROG-like method. With this method, the spatio-temporal distributions of the IAP generated in a two-color driving field have been fully characterized in both the near- and far-field in experiment, from which the spatio-temporal coupling effect during the IAP generation is evaluated. This all-optical approach has a high efficiency in the data collection, thus can be applied to characterize the IAP generated in the experiment with a low-repetition-rate laser source, where the acquisition of a photoelectron spectrum is usually time-consuming due to the space charge effects [56]. Moreover, our method is not restricted by the bandwidth of the harmonic spectrum. Since the bandwidth of the continuous harmonic spectrum in our experiment is confined by the laser conditions, we have performed simulations with a few-cycle mid-infrared laser pulse to generated broadband harmonic supercontinuum. Based on the simulations, we demonstrate that our proposed method can also be well used to characterize broadband IAPs with pulse durations less than 50 as.

Acknowledgments

This work was supported by the National Natural Science Foundation of China (91950202, 12074136, 11774109, 12021004); National Key Research and Development Program of China (2019YFA0308300); Science and Technology Planning Project of Guangdong Province (2018B090944001); Fundamental Research Funds for the Central Universities (2017KFXKJC002); Natural Science Foundation of Hubei Province (2021CFB330); and the Program for HUST Academic Frontier Youth Team.

Data availability statement

The data that support the findings of this study are available upon reasonable request from the authors.

ORCID iDs

Lixin He https://orcid.org/0000-0001-5557-9409

References

[1] Hentschel M *et al* 2001 Attosecond metrology *Nature* **414** 509
[2] Paul P, Toma E, Breger P, Mullot G, Augé F, Balcou P, Muller H and Agostini P 2001 Observation of a train of attosecond pulses from high harmonic generation *Science* **292** 1689
[3] Krausz F and Ivanov M 2009 Attosecond physics *Rev. Mod. Phys.* **81** 163
[4] Biegert J, Calegari F, Dudovich N, Quéré F and Vrakking M 2021 Attosecond technology(ies) and science *J. Phys. B: At. Mol. Opt. Phys.* **54** 070201
[5] Mashiko H, Gilbertson S, Chini M, Feng X, Yun C, Wang H, Khan S, Chen S and Chang Z 2009 Extreme ultraviolet supercontinua supporting pulse durations of less than one atomic unit of time *Opt. Lett.* **34** 3337
[6] Li J *et al* 2017 53 attosecond x-ray pulses reach the carbon K-edge *Nat. Commun.* **8** 186
[7] Gaumnitz T, Jain A, Pertot Y, Huppert M, Jordan I, Ardana-Lamas F and Wörner H 2017 Streaking of 43-attosecond soft-x-ray pulses generated by a passively CEP-stable mid-infrared driver *Opt. Express* **25** 27506
[8] Xue B, Midorikawa K and Takahashi E 2022 Gigawatt-class, tabletop, isolated-attosecond-pulse light source *Optica* **9** 360
[9] Drescher M *et al* 2002 Time-resolved atomic inner-shell spectroscopy *Nature* **419** 803
[10] Uiberacker M *et al* 2007 Attosecond real-time observation of electron tunnelling in atoms *Nature* **446** 627
[11] Schultze M *et al* 2010 Delay in photoemission *Science* **328** 1658
[12] Isinger M *et al* 2017 Photoionization in the time and frequency domain *Science* **358** 893
[13] Sansone G *et al* 2010 Electron localization following attosecond molecular photoionization *Nature* **465** 763
[14] Calegari F *et al* 2014 Ultrafast electron dynamics in phenylalanine initiated by attosecond pulses *Science* **346** 336
[15] Vos J, Cattaneo L, Patchkovskii S, Zimmermann T, Cirelli C, Lucchini M, Kheifets A, Landsman A S and Keller U 2018 Orientation-dependent stereo Wigner time delay and electron localization in a small molecule *Science* **360** 1326
[16] Cavalieri A L *et al* 2007 Attosecond spectroscopy in condensed matter *Nature* **449** 1029
[17] Corkum P B 1993 Plasma perspective on strong field multiphoton ionization *Phys. Rev. Lett.* **71** 1994
[18] Lewenstein M, Balcou P, Ivanov M, L'Huillier A and Corkum P B 1994 Theory of high-harmonic generation by low-frequency laser fields *Phys. Rev.* A **49** 2117
[19] Le A T, Lucchese R R, Tonzani S, Morishita T and Lin C D 2009 Quantitative rescattering theory for high-order harmonic generation from molecules *Phys. Rev.* A **80** 013401
[20] Gaarde M B, Tate J L and Schafer K J 2008 Macroscopic aspects of attosecond pulse generation *J. Phys. B: At. Mol. Opt. Phys.* **41** 132001
[21] Jin C, Le A T and Lin C D 2011 Medium propagation effects in high-order harmonic generation of Ar and N_2 *Phys. Rev.* A **83** 023411

[22] Wang F, He L, Zhai C, Shi W, Zhang Q, Lan P and Lu P 2015 Time-dependent phase matching of high-order-harmonic generation *Phys. Rev.* A **92** 063839
[23] Cormier E *et al* 2005 Self-referencing, spectrally, or spatially encoded spectral interferometry for the complete characterization of attosecond electromagnetic pulses *Phys. Rev. Lett.* **94** 033905
[24] Wang H, Chini M, Khan S D, Chen S, Gilbertson S, Feng X, Mashiko H and Chang Z 2009 Practical issues of retrieving isolated attosecond pulses *J. Phys. B: At. Mol. Opt. Phys.* **42** 134007
[25] Chini M, Zhao K and Chang Z 2014 The generation, characterization and applications of broadband isolated attosecond pulses *Nat. Photon.* **8** 178
[26] Kienberger R *et al* 2004 Atomic transient recorder *Nature* **427** 817
[27] Goulielmakis E *et al* 2004 Direct measurement of light waves *Science* **305** 1267
[28] Itatani J, Quéré F, Yudin G L, Ivanov M Y, Krausz F and Corkum P B 2002 Attosecond streak camera *Phys. Rev. Lett.* **88** 173903
[29] Quéré F, Mairesse Y and Itatani J 2005 Temporal characterization of attosecond XUV fields *J. Mod. Opt.* **52** 339
[30] Mairesse Y and Quéré F 2005 Frequency-resolved optical gating for complete reconstruction of attosecond bursts *Phys. Rev.* A **71** 011401
[31] Gagnon J and Yakovlev V S 2011 The direct evaluation of attosecond chirp from a streaking measurement *Appl. Phys.* B **103** 303
[32] Chini M, Gilbertson S, Khan S D and Chang Z 2010 Characterizing ultrabroadband attosecond lasers *Opt. Express* **18** 13006
[33] Keathley P D, Bhardwaj S, Moses J, Laurent G and Kärtner F X 2016 Volkov transform generalized projection algorithm for attosecond pulse characterization *New J. Phys.* **18** 073009
[34] Yu W, Zhao X, Wei H, Wang S and Lin C D 2019 Method for spectral phase retrieval of single attosecond pulses utilizing the autocorrelation of photoelectron streaking spectra *Phys. Rev.* A **99** 033403
[35] Zhao X *et al* 2020 Metrology of time-domain soft x-ray attosecond pulses and reevaluation of pulse durations of three recent experiments *Phys. Rev. Appl.* **13** 034043
[36] Zhao X *et al* 2022 Characterization of single-shot attosecond pulses with angular streaking photoelectron spectra *Phys. Rev.* A **105** 013111
[37] Zhu Z, White J, Chang Z and Pang S 2020 Attosecond pulse retrieval from noisy streaking traces with conditional variational generative network *Sci. Rep.* **10** 5782
[38] White J and Chang Z 2019 Attosecond streaking phase retrieval with neural network *Opt. Express* **27** 4799
[39] Dubrouil A, Hort O, Catoire F, Descamps D, Petit S, Mével E, Strelkov V V and Constant E 2014 Spatio-spectral structures in high-order harmonic beams generated with Terawatt 10 fs pulses *Nat. Commun.* **5** 4637
[40] Tosa V, Kim K T and Nam C H 2009 Macroscopic generation of attosecond-pulse trains in strongly ionized media *Phys. Rev.* A **79** 043828
[41] Lee D G, Park J J, Sung J H and Nam C H 2003 Wave-front phase measurements of high-order harmonic beams by use of point-diffraction interferometry *Opt. Lett.* **28** 480
[42] Frumker E, Paulus G G, Niikura H, Villeneuve D M and Corkum P B 2009 Frequency-resolved high-harmonic wavefront characterization *Opt. Lett.* **34** 3026
[43] Austin D R, Witting T, Arrell C A, Frank F, Wyatt A S, Marangos J P, Tisch J W G and Walmsley I A 2011 Lateral shearing interferometry of high-harmonic wavefronts *Opt. Lett.* **36** 1746
[44] Dudovich N, Smirnova O, Levesque J, Mairesse Y, Ivanov M Y, Villeneuve D M and Corkum P B 2006 Measuring and controlling the birth of attosecond XUV pulses *Nat. Phys.* **2** 781
[45] Kim K T, Zhang C, Shiner A D, Kirkwood S E, Frumker E, Gariepy G, Naumov A, Villeneuve D M and Corkum P B 2013 Manipulation of quantum paths for space-time characterization of attosecond pulses *Nat. Phys.* **9** 159
[46] Kane D and Trebino R 1993 Characterization of arbitrary femtosecond pulses using frequency-resolved optical gating *IEEE J. Quantum Electron.* **29** 571
[47] Kane D 1999 Recent progress toward real-time measurement of ultrashort laser pulses *IEEE J. Quantum Electron.* **35** 421
[48] Yang Z *et al* 2020 All-optical frequency-resolved optical gating for isolated attosecond pulse reconstruction *Opt. Lett.* **45** 567
[49] Takahashi E J *et al* 2013 Attosecond nonlinear optics using gigawatt-scale isolated attosecond pulses *Nat. Commun.* **4** 2691
[50] Lan P, Takahashi E J and Midorikawa K 2010 Optimization of infrared two-color multicycle field synthesis for intense-isolated-attosecond-pulse generation *Phys. Rev.* A **82** 053413
[51] Kovacs K, Tosa V, Major B, Balogh E and Varju K 2015 High efficiency single attosecond pulse generation with a long wavelength pulse assisted by a weak near infrared pulse *IEEE J. Sel. Top. Quantum Electron.* **21** 1
[52] Lan P, Takahashi E J and Midorikawa K 2010 Wavelength scaling of efficient high-order harmonic generation by two-color infrared laser fields *Phys. Rev.* A **81** 061802
[53] Queipo N, Haftka R, Shyy W, Goel T, Vaidyanathan R and Tucker P K 2005 Surrogate-based analysis and optimization *Prog. Aerosp. Sci.* **41** 1
[54] Gabolde P, Lee D, Akturk S and Trebino R 2007 Describing first-order spatio-temporal distortions in ultrashort pulses using normalized parameters *Opt. Express* **15** 242
[55] Lu C, Witting T, Husakou A, Vrakking M J J, Kung A H and Furch F J 2018 Sub-4 fs laser pulses at high average power and high repetition rate from an all-solid-state setup *Opt. Express* **26** 8941
[56] Verna A, Greco G, Lollobrigida V, Offi F and Stefani G 2016 Space-charge effects in high-energy photoemission *J. Electron. Spectrosc. Relat. Phenom.* **209** 14